Wavenumber Lock-in in Buckled Elastic Structures: An Analogue to Parametric Instabilities

H. E. Read,[1] G. Risso,[1] A. Djellouli,[1] K. Bertoldi,[1,*] and A. Lazarus[2,3,†]
[1]School of Engineering and Applied Sciences, Harvard University, Cambridge, Massachusetts 02138, USA
[2]Department of Mathematics, Massachusetts Institute of Technology, Cambridge, Massachusetts 02139, USA
[3]Institut Jean Le Rond d'Alembert, CNRS UMR7190, Sorbonne Université, Paris, France

(Received 29 August 2025; accepted 20 April 2026; published 18 May 2026)

Parametric instabilities are a known feature of periodically driven dynamic systems; at particular frequencies and amplitudes of the driving modulation, the system's quasiperiodic response undergoes a frequency lock-in, leading to a periodically unstable response. Here, we demonstrate an analogous phenomenon in a purely static context. We show that the buckling patterns of an elastic beam resting on a modulated Winkler foundation display the same kind of frequency lock-in observed in dynamic systems. Through simulations and experiments, we reveal that compressed elastic strips with modulated height alternate between predictable quasiperiodic and periodic buckling modes. Our findings uncover previously unexplored analogies between structural and dynamic instabilities, highlighting how even simple elastic structures can give rise to rich and intriguing behaviors.

DOI: 10.1103/56q8-bjw2

Introduction—Parametric instabilities are a well studied class of instability that arise in systems subjected to periodic driving. These phenomena appear across a wide range of physical systems, including pendula [1,2], surface gravity waves [3,4], wrinkled elastic sheets [5], and Floquet time crystals [6,7]. In all these systems, specific combinations of excitation frequency and amplitude cause perturbations around equilibrium to become dynamically amplified—a phenomenon known as frequency lock-in. A classic example of a system exhibiting frequency lock-in is the inverted pendulum [8,9] [Fig. 1(a) and Supplemental Material [10]]. When its base is oscillated vertically, it is well known that a statically unstable upright position can become stable for specific combinations of oscillation amplitude and frequency [18]. More generally, this Floquet system exhibits alternating stable and unstable regions in the amplitude-frequency space [19], with the unstable regions forming characteristic tonguelike shapes. These so-called instability tongues, often referred to as Arnold tongues [20], correspond to parametric resonances, where the quasiperiodic response "locks in" to become periodic, with a period either twice or equal to the driving period $\bar{T}$ [white and black regions in Fig. 1(b), respectively], while growing exponentially in time to eventually reach a limit cycle.

Another extensively studied class of instabilities is structural instabilities, such as buckling, creasing, and snapping [21]. These instabilities arise in elastic structures when compressive forces exceed a critical threshold [22], resulting in sudden and often dramatic shape changes. These phenomena have attracted considerable attention in recent years. They have been harnessed to enable functional behavior such as reconfigurable, adaptive, and extreme shape morphing [23–31], and they have served as powerful tools for probing complex physical phenomena, offering intuitive platforms to visualize effects that are otherwise difficult to observe. Examples include the amplification of chirality [32], as well as domain wall motion [33] and phase transitions [34,35]. In addition, researchers have begun to draw analogies between structural and dynamic instabilities. For instance, period-doubling bifurcations, a hallmark of nonlinear dynamic systems, have been observed in the postbuckling regime of compressed elastic structures [36,37], highlighting the rich and complex behavior of elastic systems.

Motivated by these efforts, we show that the buckling behavior of certain elastic structures can display key features typically associated with parametric resonance, most notably the emergence of frequency lock-in phenomena. To explore this analogy between parametric instabilities and structural buckling, we begin by analyzing an axially compressed beam resting on a bed of springs with spatially modulated stiffness [Fig. 1(c)]. Buckling occurs when the applied force exceeds a critical threshold, giving rise to a wavy deformation pattern corresponding to the system's critical mode. Remarkably, in close analogy to parametric instabilities, the resulting buckling modes alternate between periodic and quasiperiodic behavior depending on the amplitude and wavelength of the stiffness modulation with the periodic regions forming distinctive tonguelike shapes [Fig. 1(d)]. Building on these results, we

*Contact author: bertoldi@seas.harvard.edu
†Contact author: arnaud.lazarus@upmc.fr

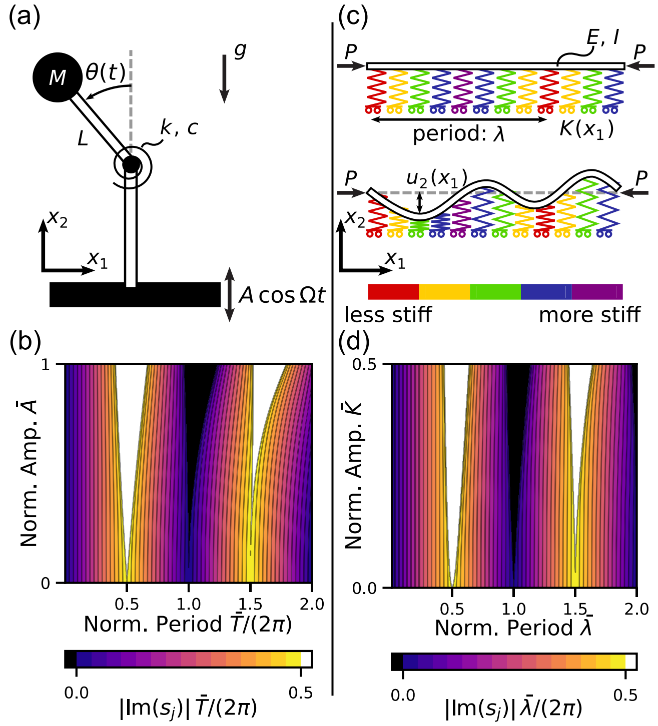

FIG. 1. Frequency lock-in in dynamics and statics. (a) An inverted parametric pendulum. (b) Maximum normalized imaginary component of Floquet exponents s_j for the inverted pendulum in the first Brillouin zone. (c) A modulated Winkler foundation. (d) Maximum normalized imaginary component of s_j for the modulated Winkler foundation.

construct a three-dimensional analogue consisting of a thin elastic strip with periodically varying height, clamped and compressed along its bottom edge. Through a combination of experiments and numerical simulations, we show that this system reproduces the essential behavior of the spring-supported beam and similarly exhibits an alternation between periodic and quasiperiodic buckling patterns that is fully governed by the geometric modulation of the strip.

A boundary value analogue—We start by considering an elastic beam with bending modulus EI on a linear Winkler foundation with a periodic stiffness per unit length [see Fig. 1(c)],

$$K(x_1) = K_0 + K_1 \cos\frac{2\pi}{\lambda}x_1, \tag{1}$$

where K_0 is the base stiffness, K_1 is the amplitude of modulation, and λ is the wavelength of modulation. The linearized equilibrium equation governing its transverse deflection $u_2(x_1)$ about the trivial flat state $u_2 = 0$ upon application of an axial load P takes the following form [37,38]:

$$u_2^{(4)} + \bar{P}u_2'' + 16\pi^4\left(1 + \bar{K}\cos\frac{2\pi}{\bar{\lambda}}\bar{x}_1\right)u_2 = 0, \tag{2}$$

where $\bar{K} = K_1/K_0$ and $\bar{P} = 4\pi^2 P/\sqrt{K_0 EI}$. Moreover, $\bar{\lambda} = \lambda/\lambda_0$ and $\bar{x}_1 = x_1/\lambda_0$, with

$$\lambda_0 = 2\pi\left(\frac{EI}{K_0}\right)^{1/4}, \tag{3}$$

which corresponds to the buckling wavelength of an inextensible Euler-Bernoulli beam resting on an unmodulated Winkler foundation (i.e., $K_1 = 0$) [37] (see [10] for details). Equation (2) shows that, much like the inverted pendulum, the response of the modulated Winkler foundation is governed by a linear differential equation with periodically varying coefficients. According to Floquet-Bloch theory [39], the solutions to such equations can be expressed in the reciprocal space as

$$\hat{y}(\bar{x}) = \sum_{j=1}^{4}\sum_{h\in\mathbb{Z}} r_j^h e^{(ih2\pi/\bar{\lambda}+s_j)\bar{x}_1}, \tag{4}$$

where $s_j \in \mathbb{C}$ are the Floquet exponents and $r_j^h \in \mathbb{C}$ are harmonics of a periodic function and are determined by boundary conditions (see [10] for details). Instead of computing the full solution, we focus on determining the Floquet exponents within the first Brillouin zone, $|\mathrm{Im}(s_j)| \le \pi/\bar{\lambda}$, using the Hill (spectral) method [40–42], as they offer key insights into the linear behavior of the system. A nontrivial bounded solution $u_2(\bar{x}_1) \neq 0$ exists whenever at least one Floquet exponent has zero real part [i.e., $\mathrm{Re}(s_j) = 0$]. Therefore, we define the critical buckling load P_{cr} as the minimum applied load at which the real part of at least one Floquet exponent vanishes. The imaginary parts of the Floquet exponents satisfying $\mathrm{Re}(s_j) = 0$ at P_{cr} reveal the spectral content of the emerging buckling mode. From Eq. (4), it follows that the wave number spectrum of $u_2(\bar{x}_1)$ is given by $\mathrm{Im}(s_j) + h2\pi/\bar{\lambda}$, where $h \in \mathbb{Z}$. If $\mathrm{Im}(s_j) = 0$, the spectrum reduces to integer multiples of $2\pi/\bar{\lambda}$, meaning the buckling mode is $\bar{\lambda}$ periodic. If $|\mathrm{Im}(s_j)| = \pi/\bar{\lambda}$, the spectrum instead reduces to half-integer multiples of $2\pi/\bar{\lambda}$, so the mode becomes $2\bar{\lambda}$ periodic. In all other cases, the buckling mode is quasiperiodic, characterized by two incommensurate wave numbers.

In Fig. 1(d) we show the evolution of the maximum $\mathrm{Im}(s_j)\bar{\lambda}/(2\pi)$ in the first Brillouin zone as a function of $\bar{\lambda}$ and $\bar{K}$ at the onset of buckling. We again see the emergence of "frequency" lock-in tongues; in these regions, the wave number response "locks in" to either double (white) or equal (black) to the "driving" wavelength $\bar{\lambda}$ of the foundation. As with the inverted pendulum, outside of these tongues, our solution is quasiperiodic.

A physical realization—The results shown in Fig. 1 reveal that the buckling modes of an elastic beam resting on a Winkler foundation with periodically modulated stiffness

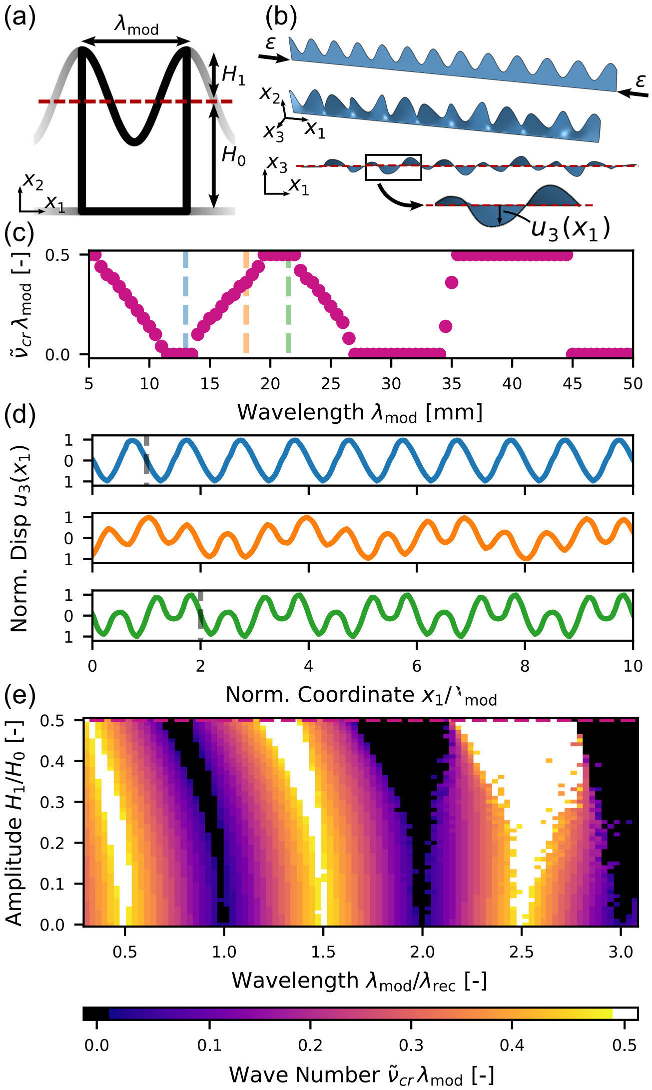

FIG. 2. Numerically predicted wave number response of the compressed elastic strip. (a) Schematic of our system. (b) When compressed along its bottom edge, the strip buckles out of plane. (c) Critical wave numbers as a function of λ_{mod} at $H_1/H_0 = 0.5$. (d) Example reconstructions; periodicity marked with the gray dashed line. (e) Wave number lock-in tongues; the horizontal slice that generates 2c is shown in magenta.

exhibit wave number lock-in tongues. Motivated by this observation, we seek to design a physical platform that reproduces the same phenomenon. Because the buckling of a modulated Winkler foundation is governed by a differential equation with periodically varying coefficients, our objective is to realize an elastic system whose response is described by a similar class of equations, while remaining straightforward to implement experimentally. To this end, we consider thin elastic plates embedded in the three-dimensional space (x_1, x_2, x_3) with thickness t in the x_3 direction, which is small compared to their characteristic dimensions in the x_1 and x_2 directions. The critical buckling load and the associated buckling mode for such plates are obtained by solving the following eigenvalue problem (see [10] for details):

$$D\nabla^4 \tilde{u}_3(\mathbf{x}) - \kappa \frac{\partial}{\partial x_\alpha}\left(t\sigma^0_{\alpha\beta}(\mathbf{x}) \frac{\partial \tilde{u}_3}{\partial x_\beta}(\mathbf{x}) \right) = 0, \tag{5}$$

where $\alpha, \beta = 1, 2$, $D = Eh^3/[12(1-\nu^2)]$ is the plate's bending stiffness, $\mathbf{x} = x_1\mathbf{e}_1 + x_2\mathbf{e}_2$ is the midsurface position vector ($\mathbf{e}_i$ denoting the Cartesian basis vectors), ∇^4 denotes the biharmonic operator with respect to $\mathbf{x}$, κ is the loading parameter, $\sigma^0_{\alpha\beta}$ is the in-plane base stress state, and $\tilde{u}_3(\mathbf{x})$ is the out-of-plane displacement defining the buckling mode.

We start by focusing on a rectangular plate that, in the reference configuration, occupies the domain $\Omega = \{0 \le x_1 \le L, 0 \le x_2 \le H_0, -t/2 \le x_3 \le t/2\}$, where L and H_0 denote the length and height of the plate, respectively, and $L \gg H_0 \gg t$. When the bottom edge ($x_2 = 0$) of the plate is uniformly compressed and constrained against transverse motion [$u_3(x_1, 0) = 0$], Eq. (5) has constant coefficients, and buckling triggers the formation of a wavy pattern with wavelength [43,44]

$$\lambda_{\mathrm{rec}} = 3.256 H_0. \tag{6}$$

If, however, the plate height is periodically modulated according to

$$H(x_1) = H_0 + H_1 \cos \frac{2\pi}{\lambda_{\mathrm{mod}}} x_1, \tag{7}$$

where H_1 is the amplitude of modulation, and λ_{mod} is the "driving" wavelength [Fig. 2(a)], the in-plane stresses $\sigma^0_{\alpha\beta}(x_1, x_2)$ become λ_{mod} periodic in x_1 (see [10] for details). Equation (5) then becomes a homogeneous partial differential equation with periodic coefficients, which is expected to exhibit wave number lock-in tongues in the $(H_1, \lambda_{\mathrm{mod}})$ modulation parameter space. Since the governing equation (5) is now a partial differential equation, we employ Bloch wave analysis [45], a three-dimensional generalization of the Floquet analysis used for the Winkler foundation, implemented within a finite-element (FE) framework to determine the critical buckling load and characterize the emerging buckling modes.

Specifically, we consider a unit cell of length λ_{mod}, which we first compress to some axial strain ϵ under periodic boundary conditions. We then investigate Bloch-type small perturbations superimposed on the axially compressed finite state of deformation,

$$\mathbf{u}^{\mathrm{right}} = \mathbf{u}^{\mathrm{left}} e^{i2\pi\tilde{\nu}\lambda_{\mathrm{mod}}}, \tag{8}$$

where $\tilde{\nu}$ is a wave number and $\mathbf{u}^{\mathrm{right}}$ and $\mathbf{u}^{\mathrm{left}}$ denote the displacement of superimposed perturbation applied to the right and left edges, respectively. Buckling is triggered at

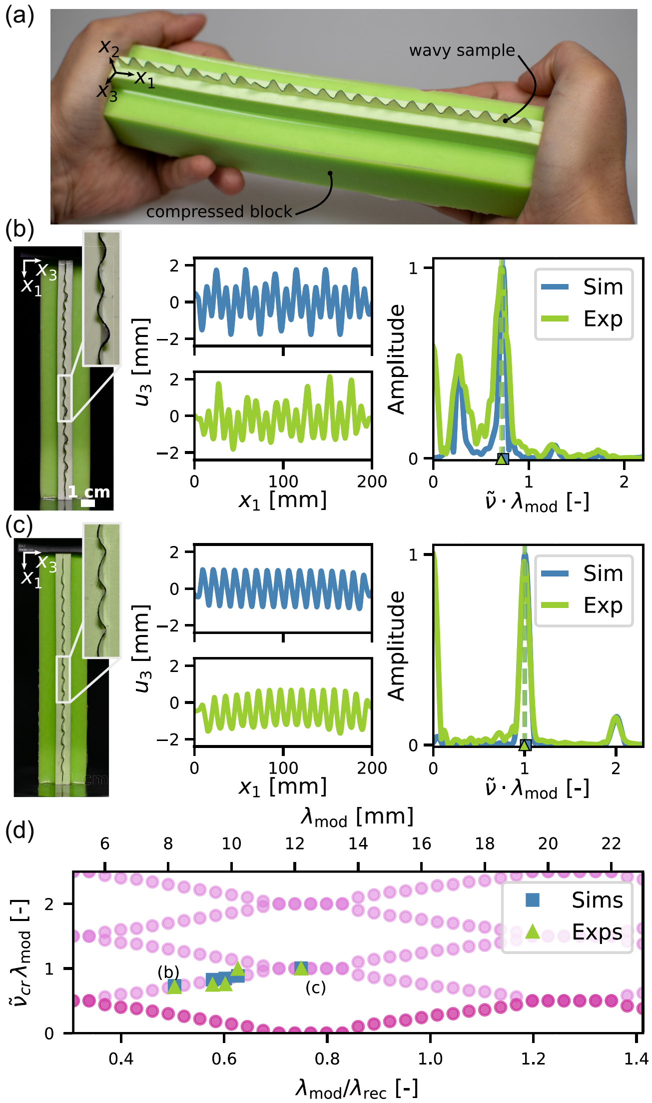

FIG. 3. Experimental analysis. (a) An experimental sample with the top edge highlighted with a black marker. We compress the larger attached block to impose uniform compressive strain along the bottom edge of the wavy plate. (b),(c) Experimental, simulation deformation and Fourier transform for (b) $\lambda_{\rm mod} = 8.2$ mm and $H_1/H_0 = 0.5$ and (c) $\lambda_{\rm mod} = 12.2$ mm and $H_1/H_0 = 0.5$. (d) Peak wave number location in postbuckling simulation vs experimental samples; Bloch wave simulation data are shown in pink.

the lowest applied strain ϵ for which a vanishing eigenfrequency exists for wave numbers $\tilde{\nu}$ within the first Brillouin zone, i.e., $\tilde{\nu} \in [0, 1/\lambda_{\rm mod})$; because of symmetry in our system, we can further restrict ourselves to $\tilde{\nu} \in [0, 0.5/\lambda_{\rm mod}]$ (see [10] for details). In Fig. 2(c), we report the calculated critical values of $\tilde{\nu}$, denoted as $\tilde{\nu}_{cr}$, as a function of $\lambda_{\rm mod}$ for a strip with $H_1/H_0 = 0.5$. As in the case of the Winkler foundation, we observe locked-in regions at $\tilde{\nu}_{cr}\lambda_{\rm mod} = 0$ and 0.5, corresponding to periodic solutions with wavelengths $\lambda_{\rm mod}$ and $2\lambda_{\rm mod}$, respectively. This is confirmed by the reconstructed buckling modes, shown in Fig. 2(d); in analogy to the transverse displacement $u_2(x_1)$ in the Winkler foundation, we display the out-of-plane displacement along the top edge $[x_2 = H(x_1)]$ of the strip, $u_3(x_1) = u_3^{\rm top}$ [Fig. 2(b)].

Finally, we compute the critical wave numbers $\tilde{\nu}_{cr}$ for 51 amplitude values in the range $H_1/H_0 \in [0, 0.5]$ and 91 modulation wavelengths $\lambda_{\rm mod} \in [5, 50]$ mm (corresponding to $\lambda_{\rm mod}/\lambda_{\rm rec} \in [0.307, 3.07]$) and present the results in Fig. 2(e). As in the case of the modulated Winkler foundation, we observe the emergence of "instability tongues," where wave number lock-in occurs and the solution becomes periodic, confirming that an axially compressed elastic strip with modulated height displays features typically associated with parametric resonance.

Guided by the results of Fig. 2, we fabricate four samples with $H_1/H_0 = 0.5$ and modulation wavelengths $\lambda_{\rm mod} =$ 8.2, 9.4, 9.8, 10.2, and 12.2 mm. Based on the Bloch wave analysis, we expect the sample with $\lambda_{\rm mod} = 12.2$ mm to exhibit a periodic postbuckling deformation with period $\lambda_{\rm mod}$, while all other samples should display quasiperiodic postbuckling deformation. The samples are cast from an elastomeric material (Zhermack Elite Double 32) using a molding process (see [10] for details). All strips have a length $L = 200$ mm, a nominal height $H_0 = 5$ mm, and thickness $t = 0.5$ mm.

To apply axial compression, each thin strip is bonded to a larger block of the same material [Fig. 3(a)], which is then compressed to induce buckling in the strip. We mark the top edge of each strip in black and track its deformation during compression. The resulting buckling patterns for $\lambda_{\rm mod} =$ 8.2 mm and $\lambda_{\rm mod} = 12.2$ mm are shown in Figs. 3(b) and 3(c), respectively. All samples were compressed to between 5–6.5% strain, which is much larger than the compressive strain needed for buckling onset (see [10] for details). As expected, the sample with $\lambda_{\rm mod} = 8.2$ mm exhibits a disordered postbuckling deformation, while the sample with $\lambda_{\rm mod} = 12.2$ mm shows an ordered, apparently periodic postbuckling pattern. To quantify these observations, we perform a discrete Fourier transform (DFT) on the experimental data. For the sample with $\lambda_{\rm mod} = 12.2$ mm, the DFT shows a spectral peak at $\tilde{\nu}\lambda_{\rm mod} = 1.0$, confirming that the deformation is periodic with a spatial period equal to $\lambda_{\rm mod}$. In contrast, the spectrum for $\lambda_{\rm mod} = 8.2$ mm exhibits a peak at $\tilde{\nu}\lambda_{\rm mod} = 0.71$, indicating that the response is quasiperiodic.

Concurrently, we perform FE simulations on strips of the same dimensions used in the experiments ($L = 200$ mm). As in the experiments, the models are compressed into the postbuckling regime, with the first linear buckling mode introduced as a geometric imperfection to initiate the instability (see [10] for details). As shown in Figs. 3(b) and 3(c), we observe good agreement between simulations and experiments, both qualitatively and quantitatively, in the out-of-plane deformation of the top edge.

Finally, we compare these results with those obtained from the Bloch wave analysis, theoretically valid for an infinite strip length. In Fig. 3(d), the magenta markers indicate the values of $\tilde{\nu}_{cr}\lambda_{\mathrm{mod}}$ predicted by the Bloch analysis (same data as in Fig. 2(c), but here we also display the extended region in a lighter shade), while the blue and green markers represent the dominant DFT peaks extracted from the numerical simulations and experimental data, respectively. We observe good overall agreement between the experimental and numerical results, demonstrating that the transition from quasiperiodic to periodic behavior is accurately captured even for the relatively short strip length used in our study. Importantly, this agreement is not limited to the two representative cases shown in Figs. 2(b) and 2(c) but also holds across the three additional tested samples (see [10] for details).

In summary, we have demonstrated the realization of a static analog of parametric instabilities. We first established this in the archetypal case of a beam on a modulated Winkler foundation, where Floquet analysis revealed the same frequency lock-in tongues that characterize dynamic systems exhibiting parametric instabilities. We then extended the concept to a physical platform: an elastic plate with modulated height. Using a combination of Bloch wave analysis and experiments, we again observed the characteristic lock-in tongues, confirming the predictable alternation between quasiperiodic and fully periodic buckling patterns. As such, this work sheds light on the analogy between boundary value problems (BVPs) in elasticity and initial value problems (IVPs) in classical dynamical systems. Nevertheless, important conceptual differences remain between IVPs and BVPs. In IVPs, solutions evolve uniquely in time, with linear responses typically decaying or diverging under parametric excitation until nonlinear effects give rise to limit cycles. In contrast, in BVPs, nontrivial buckled solutions emerge at critical parameter values when the trivial state loses stability. Consequently, BVPs naturally admit bounded periodic or quasiperiodic equilibrium solutions, whereas in IVPs dissipation and temporal evolution determine whether energy is amplified or absorbed. The wave number lock-in phenomenon uncovered in this paper in the framework of elastic buckling should offer promising opportunities, for example, in the spectral enrichment of elastic wrinkling patterns [29,46–48]. For the wrinkling pattern modulation to be real time, one could control the underlying periodic geometry with programmable and active elastic metamaterials [49–51]. Another promising direction is to extend the analogy with parametric instabilities, where recent work has shown that, in a certain modulation regime, Floquet-Bloch theory becomes mathematically equivalent to the linear algebra of quantum mechanics [52,53]—opening new opportunities for exotic functionalities in buckled elastic systems.

Acknowledgments—This work was supported by the Simons Collaboration on Extreme Wave Phenomena Based on Symmetries. G. R. acknowledges support from the Swiss National Science Foundation under Grant No. P500PT-217901. A. L. acknowledges support from the French National Center for Scientific Research for hosting him in a CNRS delegation.

Data availability—The data that support the findings of this study are openly available in [54], embargo periods may apply.

[1] J. R. Sanmartín Losada, Am. J. Phys. **52**, 937 (1984).
[2] A. A. Grandi, S. Protière, and A. Lazarus, Extreme Mech. Lett. **43**, 101195 (2021).
[3] M. Faraday, Phil. Trans. R. Soc. London **121**, 299 (1831).
[4] T. B. Benjamin and F. J. Ursell, Proc. R. Soc. A **225**, 505 (1954).
[5] H. Diamant, Eur. Phys. J. E **44**, 78 (2021).
[6] T. L. Heugel, M. Oscity, A. Eichler, O. Zilberberg, and R. Chitra, Phys. Rev. Lett. **123**, 124301 (2019).
[7] J. Zhang, P. W. Hess, A. Kyprianidis, P. Becker, A. Lee, J. Smith, G. Pagano, I.-D. Potirniche, A. C. Potter, A. Vishwanath *et al.*, Nature (London) **543**, 217 (2017).
[8] H. Smith and J. A. Blackburn, Am. J. Phys. **60**, 909 (1992).
[9] D. J. Acheson and T. Mullin, Nature (London) **366**, 215 (1993).
[10] See Supplemental Material at http://link.aps.org/supplemental/10.1103/56q8-bjw2 for details on: (i) modeling of the parametric pendulum; (ii) derivation of the modulated Winkler foundation problem; (iii) Floquet theory formulation; (iv) theory of an elastic strip with modulated height; (v) finite element simulations; (vi) experimental fabrication procedures; (vii) experimental testing procedures, which includes Refs. [11–17].
[11] A. Lazarus, C. Maurini, and S. Neukirch, in *Extremely Deformable Structures* (Springer, New York, 2015), Chap. 1, pp. 1–53.
[12] R. A. Calico and W. E. Wiesel, J. Guidance Control Dyn. **7**, 671 (1984).
[13] J. Zhou, T. Hagiwara, and M. Araki, Systems and Control Letters **53**, 141 (2004).
[14] S. P. Timoshenko and S. Woinowsky-Krieger, *Theory of Plates and Shells* (McGraw-Hill, New York, 1959).
[15] P. G. Ciarlet, J. Elast. **78**, 1 (2005).
[16] J. Liu and K. Bertoldi, Proc. R. Soc. A **471**, 20150493 (2015).
[17] M. Åberg and P. Gudmundson, J. Acoust. Soc. Am. **102**, 2007 (1997).
[18] *Collected Papers of P.L. Kapitza*, edited by D. Ter Haar (Pergamon, 1965), pp. 714–725, 10.1016/B978-0-08-010973-2.50015-X.
[19] A. A. Grandi, S. Protière, and A. Lazarus, Nonlinear Dyn. **111**, 12339 (2023).
[20] V. I. Arnold, *Ordinary Differential Equations* (Springer Science & Business Media, New York, 1992).

[21] B. Audoly and Y. Pomeau, in *Peyresq Lectures on Nonlinear Phenomena* (World Scientific, Singapore, 2000), pp. 1–35.
[22] Z. P. Bazant and L. Cedolin, *Stability of Structures: Elastic, Inelastic, Fracture and Damage Theories* (World Scientific, Singapore, 2010).
[23] K. Krieger, Nat. News **488**, 146 (2012).
[24] P. M. Reis, J. Appl. Mech. **82**, 111001 (2015).
[25] J. Shim, C. Perdigou, E. R. Chen, K. Bertoldi, and P. M. Reis, Proc. Natl. Acad. Sci. U.S.A. **109**, 5978 (2012).
[26] A. Lazarus and P. M. Reis, Adv. Eng. Mater. **17**, 815 (2015).
[27] G. Risso, M. Sakovsky, and P. Ermanni, Compos. Struct. **268**, 113946 (2021).
[28] Y. Yang, H. Read, M. Sbai, A. Zareei, A. E. Forte, D. Melancon, and K. Bertoldi, Adv. Mater. **36**, 2406611 (2024).
[29] E. Lee, M. Zhang, Y. Cho, Y. Cui, J. Van der Spiegel, N. Engheta, and S. Yang, Adv. Mater. **26**, 4127 (2014).
[30] O. Doaré and S. Michelin, J. Fluids Struct. **27**, 1357 (2011).
[31] S. Michelin and O. Doaré, J. Fluid Mech. **714**, 489 (2013).
[32] S. H. Kang, S. Shan, W. L. Noorduin, M. Khan, J. Aizenberg, and K. Bertoldi, Adv. Mater. **25**, 3380 (2013).
[33] B. Deng, S. Yu, A. E. Forte, V. Tournat, and K. Bertoldi, Proc. Natl. Acad. Sci. U.S.A. **117**, 31002 (2020).
[34] L. Jin, R. Khajehtourian, J. Mueller, A. Rafsanjani, V. Tournat, K. Bertoldi, and D. M. Kochmann, Proc. Natl. Acad. Sci. U.S.A. **117**, 2319 (2020).
[35] N. Nadkarni, A. F. Arrieta, C. Chong, D. M. Kochmann, and C. Daraio, Phys. Rev. Lett. **116**, 244501 (2016).
[36] F. Brau, H. Vandeparre, A. Sabbah, C. Poulard, A. Boudaoud, and P. Damman, Nat. Phys. **7**, 56 (2011).
[37] F. Brau, P. Damman, H. Diamant, and T. A. Witten, Soft Matter **9**, 8177 (2013).
[38] R. Lagrange and D. Averbuch, Int. J. Mech. Sci. **63**, 48 (2012).
[39] J. A. Richards, *Analysis of Periodically Time-Varying Systems* (Springer Science & Business Media, New York, 2012).
[40] G. W. Hill, Acta Math. **8**, 3 (1886).
[41] B. Deconinck, F. Kiyak, J. D. Carter, and J. N. Kutz, Math. Comput. Simul. **74**, 370 (2007).
[42] B. Bentvelsen and A. Lazarus, Nonlinear Dyn. **91**, 1349 (2018).
[43] T. Mora and A. Boudaoud, Eur. Phys. J. E **20**, 119 (2006).
[44] E. Siéfert, N. Cattaud, E. Reyssat, B. Roman, and J. Bico, Phys. Rev. Lett. **127**, 168002 (2021).
[45] L. Brillouin, *Wave Propagation in Periodic Structures* (McGraw-Hill, New York, 1946), 1st ed.
[46] X. Chen and J. W. Hutchinson, J. Appl. Mech. **71**, 597 (2004).
[47] H. Lee, J. G. Bae, W. B. Lee, and H. Yoon, Soft Matter **13**, 8357 (2017).
[48] D. Wu, Y. Huang, Q. Zhang, P. Wang, Y. Pei, Z. Zhao, and D. Fang, J. Mech. Phys. Solids **162**, 104838 (2022).
[49] C. Löwe, X. Zhang, and G. Kovacs, Adv. Eng. Mater. **7**, 361 (2005).
[50] B. Florijn, C. Coulais, and M. van Hecke, Phys. Rev. Lett. **113**, 175503 (2014).
[51] A. Ghatak, M. Brandenbourger, J. Van Wezel, and C. Coulais, Proc. Natl. Acad. Sci. U.S.A. **117**, 29561 (2020).
[52] A. Lazarus and E. Trélat, Phys. Rev. E **113**, 034204 (2026).
[53] A. Lazarus and E. Trélat, arXiv:2507.13125.
[54] H. E. Read, G. Risso, A. Djellouli, K. Bertoldi, and A. Lazarus, Data for “Wavenumber lock-in in buckled elastic structures: an analogue to parametric instabilities,” https://github.com/bertoldi-collab/wavenumber-locking (2026).